

# Projection-Based 3D Printing of Cell Patterning Scaffolds with Multiscale Channels

Dai Xue,<sup>‡,||</sup> Yancheng Wang,<sup>\*,†,‡,‡,‡</sup> Jiaxin Zhang,<sup>§</sup> Deqing Mei,<sup>†,‡</sup> Yue Wang,<sup>‡</sup> and Shaochen Chen<sup>||</sup>

<sup>†</sup>State Key Laboratory of Fluid Power and Mechatronics Systems and <sup>‡</sup>Key Laboratory of Advanced Manufacturing Technology of Zhejiang Province, School of Mechanical Engineering, Zhejiang University, Hangzhou 310027, China

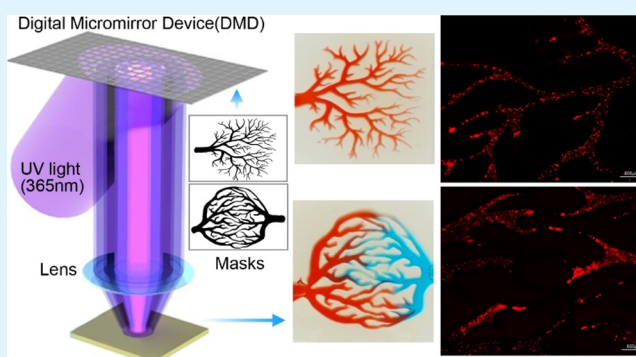
<sup>§</sup>Department of Toxicology, Fourth Military Medical University, Xi'an 710032, China

<sup>||</sup>Department of NanoEngineering, University of California, San Diego, California 92093, United States

## S Supporting Information

**ABSTRACT:** To fully actualize artificial, cell-laden biological models in tissue engineering, such as 3D organoids and organs-on-a-chip systems, cells need to be patterned such that they can precisely mimic natural microenvironments in vitro. Despite increasing interest in this area, patterning cells at multiscale ( $\sim 10\ \mu\text{m}$  to 10 mm) remains a significant challenge in bioengineering. Here, we report a projection-based 3D printing system that achieves rapid and high-resolution fabrication of hydrogel scaffolds featuring intricate channels for multiscale cell patterning. Using this system, we were able to use biocompatible poly(ethylene glycol)diacrylate in fabricating a variety of scaffold architectures, ranging from regular geometries such as serpentine, spiral, and fractal-like to more irregular/intricate geometries, such as biomimetic arborescent and capillary networks. A red food dye solution was able to freely fill all channels in the scaffolds, from the trunk ( $>1100\ \mu\text{m}$  in width) to the small branch ( $\sim 17\ \mu\text{m}$  in width) without an external pump. The dimensions of the printed scaffolds remained stable over 3 days while being immersed in Dulbecco's phosphate-buffered saline at 37 °C, and a penetration analysis revealed that these scaffolds are suitable for metabolic and nutrient transport. Cell patterning experiments showed that red fluorescent protein-transfected A549 human nonsmall lung cancer cells adhered well in the scaffolds' channels, and showed further attachment and penetration during cell culture proliferation.

**KEYWORDS:** projection-based 3D printing, hydrogel scaffold, multi-scale channel, cell patterning, cell culturing



## 1. INTRODUCTION

In native tissues and organs, cells are precisely arranged in three-dimensional (3D) spatial architectures, or microenvironments—these cell microenvironments play critical roles in facilitating healthy biological functions, such as promoting cell–cell signaling and substance exchange, as well as other interactions between cells and the extracellular matrix (ECM).<sup>1,2</sup> On-demand recapitulation of the cell microenvironment to complement native physiology is one of the key challenges in engineering tissues.<sup>3,4</sup> Besides the issue of biocompatible materials, the basic requirement for tissue-engineered constructs to be considered functional is multiscale cell patterning through fabricated scaffolds with internal architectures.<sup>5–7</sup> Typically, macroscale channels and/or pores can be used to accommodate cell attachment and growth, whereas microscale rough surfaces can improve growth factor release and nutrient transport to surrounding cells.<sup>8,9</sup>

Recent research on engineered scaffolds such as organ-on-a-chip systems,<sup>10–12</sup> hepatic models,<sup>13–15</sup> and blood vessels<sup>16–18</sup> shows promise; however, there are still challenges in precisely fabricating cell-laden, biomimetic scaffolds with multiscale

architectures varying in scale from  $10\ \mu\text{m}$  to 10 mm. This specific range spanning 3 orders of magnitude is particularly relevant to human tissues, such as liver lobules, cardiovascular, and kidney nephrons. For this reason, research on patterning cells into multiscale architectures through artificial scaffolds for biological applications, including drug discovery, cellular research, and organ engineering, have become increasingly significant.

Many methods can be used to fabricate cell patterning scaffolds, including lithography,<sup>19–21</sup> microcontact printing,<sup>22,23</sup> and additive manufacturing.<sup>24–26</sup> In particular, 3D printing has also been considered an effective method of fabricating scaffolds for either direct or indirect cell patterning because of its printing versatility and biocompatible material choices.<sup>27–29</sup> To date, extrusion-based printing has been shown to be able to print and pattern multiple cells in 3D.<sup>30,31</sup> However, because of its serialized “line-by-line” mode

**Received:** March 8, 2018

**Accepted:** May 21, 2018

**Published:** May 21, 2018

of operation, extrusion-based printing is time consuming when used to fabricate large scaffolds with complex microstructures. Other parameters such as dispensing nozzle size, motor speed, and printing pressure can also limit extrusion-based 3D printing's ability to print scaffolds at differing resolutions. Alternatively, projection-based 3D printing adopts a digital light processing (DLP) system to modulate light at the microscale and can print scaffolds in a continuous layer-by-layer fashion.<sup>32–34</sup> Because of the advantages of high printing speed and resolution, projection-based printing has been applied for the fabrication of microfluidic devices<sup>35–37</sup> and functional materials and structures.<sup>38–40</sup> When incorporated with cells and biocompatible materials, projection-based printing also has been adopted to fabricate user-defined cell laden and encapsulated scaffolds with complex structures that mimic the extracellular microenvironments.<sup>41,42</sup> In a projection-based 3D printing system, a digital micromirror device (DMD) chip displays digital models or masks through an array of millions of individually controllable reflective micromirrors, thus allowing the patterning of light in entire 2D planes on a pixel-by-pixel basis. Combining this light projection with photosensitive biomaterials enables facile photopolymerization printing of complex 3D structures, thus making projection-based 3D printing a biocompatible fabrication method with high speed and resolution. The printing speed and resolution are mainly dependent on the photosensitive materials property and the projected pixel size in the DMD chip, which can be modified by the photoinitiator and optical system in the printer.<sup>43</sup>

In this study, we present a customized projection-based 3D printing system capable of fabricating the hydrogel scaffolds with intricate channels, to be used for patterning cells on multiscale. Using this system, different scaffolds were printed through digital masks and a single light exposure step. To first demonstrate the versatility of this technique, digital masks of serpentine, spiral, and fractal patterns with variable channel widths were designed and printed. Following those, we printed bioinspired arborescent and capillary network with irregular bifurcations and intricate channels, whose widths varied from over 1 mm to about 17  $\mu\text{m}$ . Furthermore, red food dye solutions were perfused at the inlet channels of the arborescent and capillary network scaffolds to assess connectivity and demonstrate capillary force-driven perfusion. This is a feature that distinguishes our printed scaffolds relative to others, where a syringe or pump is usually required for fluid perfusion.<sup>44,45</sup> The 3 days channel stability of Dulbecco's phosphate-buffered saline (DPBS)-immersed scaffolds was then assessed, showing that no margin design or chemical modifications were needed to prevent swelling and deformation. Moreover, the potential applicability of these scaffolds for biological applications was demonstrated by penetration analysis, which indicated that nutrient and metabolite transport would proceed normally. Red fluorescent protein (RFP)-transfected A549 human nonsmall lung cancer cells were seeded in the printed arborescent and capillary network scaffolds. Fluorescent images showed that cells could diffuse into most channels after perfusion. Finally, rapid proliferation of cells in our printed scaffolds was observed via Cell Counting Kit (CCK)-8 testing, revealing the capability for cell proliferation and patterning on multiscale.

## 2. MATERIALS AND METHODS

**2.1. Material Preparation.** Water-soluble hydrogel poly(ethylene glycol)diacrylate (PEGDA, Sigma, USA) was chosen as the

prepolymer. The biocompatibility of the PEGDA for cell encapsulation and culturing through 3D printing has been demonstrated, and indeed the PEGDA with higher molecular weight ( $M_n = 3400$ ) has better biocompatibility.<sup>46</sup> The biological applications of the PEGDA with medium and lower molecular weight ( $M_n = 700$  or less) have also been conducted. The long-term mechanical property and cell viability of the PEGDA ( $M_n = 575$ ) hybrid-gel scaffolds by stereolithography has been confirmed.<sup>47</sup> In our work, the PEGDA ( $M_n = 700$ ) was used, and this material has been printed into cell-encapsulated constructs for cartilage tissue engineering and demonstrated that no harm to the tissues was done.<sup>48</sup> Lithium phenyl-2,4,6-trimethylbenzoylphosphinate (LAP) was used as the photoinitiator to crosslink PEGDA under 365 nm ultraviolet exposure. Relative to commercial photoinitiators such as 1-[4-(2-hydroxyethoxy)-phenyl]-2-hydroxy-2-methyl-1-propanone (Irgacure 2959, Sigma, USA), the time required to fully cross-link polymer by LAP is much lower. In our case, it takes 5 s to fully cross-link the polymer with the photoinitiator of LAP but will increase to more than 15 s if Irgacure 2959 is adopted instead. LAP was prepared as previously described.<sup>49</sup> Briefly, 2,4,6-trimethylbenzoyl chloride (Sigma) was added dropwise to continuously stirred dimethyl phenylphosphonite (Sigma) at room temperature and under argon. After stirring for 18 h, the excess of lithium bromide in 2-butanone solution was added to this mixture, and the resulting solution was heated to 50  $^{\circ}\text{C}$ . When solid precipitate had formed (after 10 min), the solution was cooled to room temperature and filtered. The unreacted lithium bromide in the LAP filtrate was removed by washing and filtering with 2-butanone three times. The filtrate was then transferred to a vacuum oven to remove the residual 2-butanone. The prepolymer and photoinitiator were dissolved in DPBS at a final concentration of 20% (v/v) PEGDA and 0.5% (w/v) LAP.

**2.2. Projection-Based 3D Printing System Setup.** The projection-based 3D printing system consists of three main components: the DLP system (DLP 9500UV, Texas Instruments, USA), a 365 nm UV-LED light source (LC-L1, Hamamatsu, Japan), and an optical lens (Thorlabs, USA), as shown in Figure 1. The digital

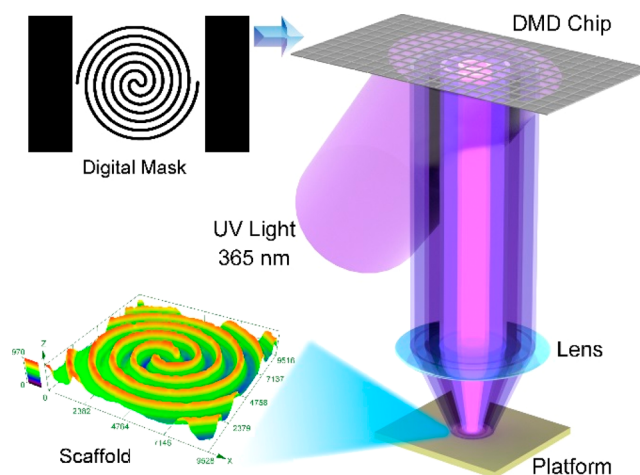


**Figure 1.** Schematic of the projection-based 3D printing system. Micromirror array is activated according to the input digital mask (.bmp images). A UV light (365 nm) illuminates the DMD chip and a modulated light pattern is generated. The light pattern is projected through a lens and focused onto the platform, where the photosensitive PEGDA solution is cross-linked.

masks (formatted as .bmp images) were loaded to the DLP system as a virtual mask sequence, thus enabling dynamic manipulation of the DMD chip's reflective mirror array to modulate incoming light and generate light patterns.<sup>50</sup> The initial UV light is expanded and collimated by the lens, and its output was adjusted to match the DMD micromirror array's reflection angle. The UV light, now reflected and modulated by the DMD chip, thus becomes a 2D light pattern, which can then be projected through a planoconvex lens onto our

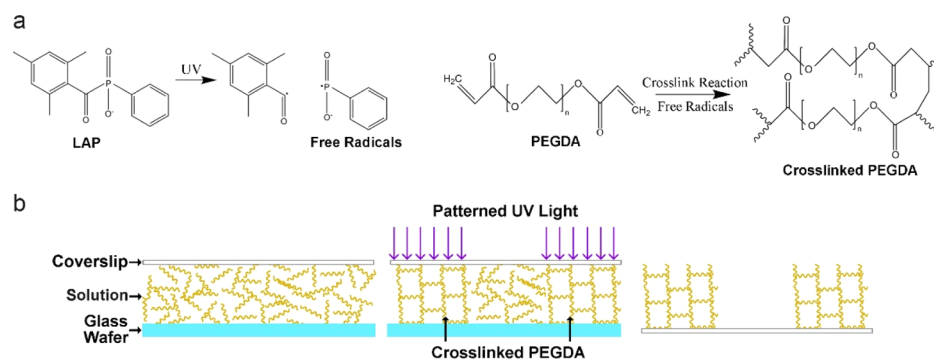


**Figure 2.** (a) Schematic for the generation of free radicals from LAP, and the free-radical-induced cross-linking of PEGDA monomers. (b) Schematic view of the printing procedure.

photosensitive PEGDA solution. The solution then selectively cures based on where the UV light pattern strikes, so that the exposed areas are cross-linked and the non-exposed areas remain liquid. The optical path was adjusted for 1:1 ratio, which means the UV light reflected by one mirror on DMD chip (one pixel on mask), is about  $10.8 \times 10.8 \mu\text{m}^2$  after being projected on the printing platform. Ideally, the printed feature sizes should be equal to the sizes on mask. To guarantee surface flatness and to avoid contact with oxygen, the photosensitive PEGDA solution is placed between a glass coverslip and a glass wafer. The printed PEGDA scaffold was firmly attached on the glass coverslip. In this case, surface treatments were needed for both the coverslip and the wafer, and detailed descriptions of these procedures are provided in Section 2.3. Additionally, the projection ratio and resolution of the UV light pattern was adjustable via the position of the planoconvex lens and the distance from the DMD chip to the PEGDA solution, meaning that the resolution of this projection-based 3D printing system is highly versatile.

**2.3. Surface Treatment of Glass Coverslip and Wafer.** To enhance adhesion between photopolymerized PEGDA and the glass coverslip, we performed a methacrylation procedure on the coverslip itself. First, glass coverslips were immersed into 10% (w/v) NaOH solution for 30 min and washed in deionized water, 75% (v/v) ethanol, and 100% ethanol (performed twice for 3 min for each wash). The coverslip was subsequently dried using nitrogen. The dried coverslips then underwent methacrylation by bathing in a solution comprised of a 85 mM 3-(trimethoxysilyl)propyl methacrylate (Sigma) ethanol solution with acetic acid (pH 4.5) for 12 h. Finally, the coverslips were washed with ethanol three times and baked for 1 h at  $100^\circ\text{C}$ .<sup>4</sup> Polydimethylsiloxane (Sylgard 184 Silicone Elastomer Kit, Dow Corning, USA) prepolymer, containing the silicone elastomer and curing agent at the weight ratio of 10:1, was spin-coated on glass wafers and cured for 4 h at  $80^\circ\text{C}$ , forming a nonstick surface layer.

**2.4. Fabrication of Cell Patterning Scaffolds.** The photosensitive polymer used here polymerizes via free-radical-based photopolymerization, where incident UV light causes free-radical generation from the photoinitiator LAP, as shown in Figure 2a. The generated free radicals activate PEGDA monomers to form cross-linked PEGDA, as seen in Figure 2b. Thus, liquid prepolymer PEGDA can be photopolymerized into a solid state through these two reactions. For the projection-based printing process, the amount and generation rate of free radicals would have significant effects on the printed thickness,<sup>51,52</sup> and the free radicals are controlled by UV power density and exposure time. To precisely control the printed thickness, the relationship between UV power density, exposure time, and thickness has been studied (Supporting Information, Figure S2). According to Figure S2b, we can precisely design and control the scaffold's thickness by selecting appropriate UV power density and exposure time. Scaffold masks were either designed using computer-aided design software (AutoCAD), such as in the case of the serpentine, spiral, and fractal-like scaffolds (Supporting Information, Figure S3) or acquired from pictures and processed digitally using imaging software (Adobe Photoshop), such as in the case of the arborescent and capillary network scaffolds. A power meter (UV-365A,

KUHNAST, Germany) was used to measure UV intensity; scaffolds were printed via exposure of liquid PEGDA to patterned UV light at an intensity of  $2.7 \text{ mW}/\text{cm}^2$ . After 2.6 s of exposure to the UV light, the PEGDA monomers in the illuminated areas were fully cross-linked. The coverslip was then transferred, and the un-crosslinked PEGDA was removed by washing with DPBS, as demonstrated in Figure 2b. The printed scaffolds together with the coverslip were maintained in DPBS before characterization and cell seeding.

**2.5. Characterization of Printed Scaffolds.** A laser confocal microscope (OLS 4100, Olympus, Japan) was used to acquire the bright-field and spatial morphology images of the printed scaffolds. Images were initially taken using the  $5\times$  objective and four individual captures of different areas of the scaffold were then stitched together to make larger coherent images. Measurements and image stitching were performed using the microscope system's provided software. To illustrate the ability of perfusion and connectivity, timelapse images were acquired during perfusion of red and blue dye solutions into the scaffolds.

Scaffold swelling, as it is often considered to be a contributor to scaffold deformation when storing them in liquids such as DPBS or culture media.<sup>29,53</sup> Significant scaffold deformation may require margin design or surface modifications to compensate for the distortion. Swelling analyses were performed on a specific channel in the network capillary scaffold, which was immersed in DPBS for 3, 6, 12, 24, and 48 h at room temperature. At each time point, scaffolds were removed from DPBS, dried, and the width was measured by the laser confocal microscope ( $n = 5$ ). A red dye solution was perfused into the capillary network scaffold, and the dye penetration process at a bifurcation was captured by the microscope.

**2.6. Cell Culture and Seeding in the Scaffolds.** RFP-transfected A549 cells (Shanghai Institute for Biological Sciences, China) were cultured in RPMI 1640 culture medium supplemented with 10% fetal bovine serum (Hyclone, USA) and 100 mg/mL penicillin–streptomycin. These cells were maintained in a humidified incubator at  $37^\circ\text{C}$  with 5%  $\text{CO}_2$ , with media changes every two days and cell passages according to protocol. Before perfusion of any printed scaffolds, they were immersed in 75% ethanol solution and subsequently washed with DPBS and RPMI 1640 culture medium three times. Once the A549 cells reached the logarithmic growth phase, they were digested by 0.25% trypsin–EDTA, and a cell suspension at a density of  $1 \times 10^5$  cell/mL was prepared for perfusing and seeding. Cell seeding was carried out by using a pipette to transfer the A549 cell suspension on the trunk inlet of scaffolds until the whole channel was immersed. The scaffolds were then covered with RPMI 1640 culture medium and maintained in the incubator for static culture. The media was changed every two days. An inverted microscope (CKX 41, Olympus, Japan) was used to observe cell morphology together with the scaffolds. Cell viability was assessed at 1, 4, 8, 12, 24, 36, and 48 h after cell seeding via a CCK-8. Fluorescent images were taken by EVOS fl imaging system (using the  $4\times$  and  $10\times$  objectives, Invitrogen, USA).

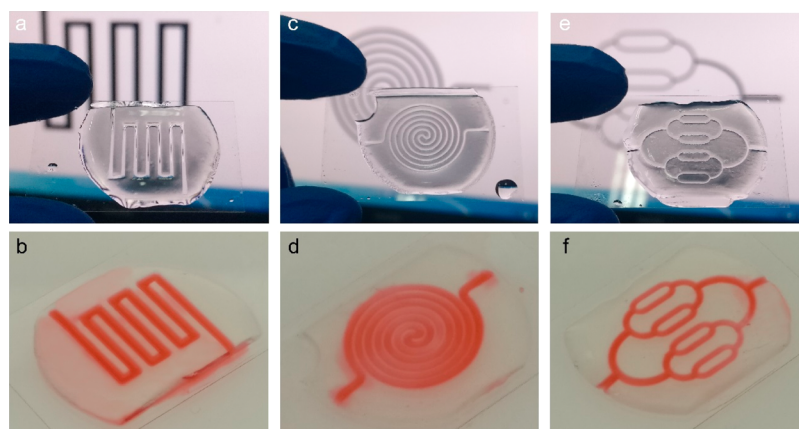


**Figure 3.** Printed scaffolds and perfusion results in (a,b) serpentine, (c,d) spiral, and (e,f) fractal scaffolds.

### 3. RESULTS AND DISCUSSION

**3.1. Printing and Characterization of Scaffolds.** A DMD chip can generate virtual masks on the basis of user-defined pictures and can be used to pattern UV light and selectively cross-link photosensitive polymers, thus facilitating printing. The two tilt angles ( $+12^\circ$  and  $-12^\circ$ ) of more than two million micromirrors on the DMD chip can be independently controlled by the pixels of the digital mask, where white/black pixels on the digital mask lead to  $+12^\circ/-12^\circ$  tilting, respectively. The UV light, only reflected by a  $+12^\circ$  tilting micromirror, is projected through the lens, ultimately cross-linking the PEGDA monomers. It is worth noting that all of the scaffolds were printed under single, short time exposure step ( $\sim 3$  s).

To demonstrate the system's printing versatility and applicability, we printed scaffold patterns seen widely used in lab-on-a-chip systems, such as the serpentine, spiral, and fractal-like patterns.<sup>29,30</sup> Printed scaffolds are illustrated in Figure 3a,c,e, with red dye perfusion demonstrated in Figure 3b,d,f. The channel width in the serpentine and spiral scaffolds is 500 and 300  $\mu\text{m}$ , respectively; the widths in the fractal scaffold are 500  $\mu\text{m}$  for the trunk, and 300, 220, and 150  $\mu\text{m}$  for the subsequent fractal levels. For mold-replica and micro-contact printing, the longer fabrication period is inevitable because of the physical mold design and fabrication. In our work, the complex scaffolds are designed from the image files, and less than 3 s is needed to print the whole scaffold. Therefore, projection-based printing process has higher versatility than other processes.

Figure 4 highlights the capability of this system as a high-resolution and versatile method to print scaffolds with intricate channels. Two different digital masks showcasing irregular-type features were used to print arborescent and capillary network scaffolds. These geometries were chosen due to the way they mimic natural fractals of varying length scales, such as those that can be seen in tree branches, leaf veins, and blood capillaries. The arborescent scaffold shown in Figure 4a, is composed of curved channels that bifurcate at various angles from the previous channels, where the channel width narrows as the number of bifurcations increase. The width of the trunk is about 900  $\mu\text{m}$ , and the minimum, found at the terminus, is about 20  $\mu\text{m}$ . This range in dimension is consistent with the variation found in native blood vessels, which vary in size from tens of microns to several millimeters in diameter. Natural derived structural design and fabrication of cell culturing chip

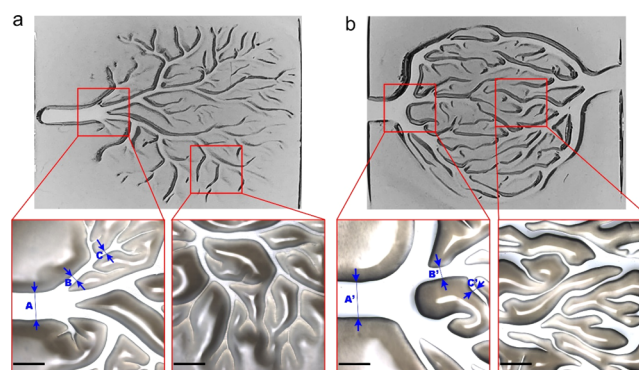


**Figure 4.** Optical images of whole and details of printed (a) arborescent and (b) capillary network scaffolds. In the zoomed images, the white regions are channels, and others are cross-linked PEGDA. A, B, C and A', B', C' are the measured position. Scale bar is 1 mm.

has been confirmed to achieve multiscale cell patterning. The pattern of the leaf veins, irregular bifurcations, and intricate channels can be precisely transferred onto the biocompatible material and applied for cell culturing.<sup>54</sup> However, several processes are required to obtain the leap mold, and the mold is hard to be modified after fabrication. In our method, only one digital mask and single-step exposure are involved for printing the scaffolds with intricate channels, and the mask is acquired from the user-defined images which expand the versatility of this method.

Figure 4b shows a biomimetic capillary network scaffold with bilateral gradient channels. Here, the trunk bifurcates into smaller branches connected in the center. These features mimic the critical features found in actual vasculature, where capillaries narrow to optimize nutrient and waste transport. The trunk is about 1100  $\mu\text{m}$  in width, and the smallest branch is 30  $\mu\text{m}$ . To compare the fabricated and designed scaffolds, three different channels (A, B, and C) in the arborescent scaffold and the other three channels (A', B', and C') are selected and marked in Figure 4. The designed and measured widths of these channels are listed in Table 1. We can see that the discrepancies from the measured widths to the designed values are in the range of 3.4–6.5%. Because of a slight over-curing, the widths of the printed channels are generally smaller than that of the designed values, while the small discrepancies between the measured and designed widths demonstrated that the proposed projection-based printing process has relatively excellent accuracy and resolution.

**Table 1. Widths Comparison between the Designed and Printed Channels**

		designed ( $\mu\text{m}$ )	printed ( $\mu\text{m}$ )	deviation (%)
arborescent scaffold	A	896.4	861.3	3.9
	B	194.4	181.6	6.5
	C	97.2	92.1	5.1
capillary network scaffold	A'	1155.0	1114.8	3.4
	B'	345.6	329.5	4.6
	C'	140.4	135.0	3.8

Unlike other active perfusions, which require a syringe or pump, the channels in both arborescent and capillary network scaffolds shown here are perfused through passive capillary action alone. Despite the many subtle bifurcations and channels found in both tree-like and capillary-like scaffolds, every channel is fully perfused when dye solutions are dropped at the inlet and outlet. We showcase this perfusion connectivity in Figure 5.

A feature of PEGDA that contributes to its biocompatibility is its degree of porosity—such porosity benefits nutrient transport and cell viability. In addition, the molecular weight of the PEGDA monomers has also been shown to influence porosity: porosity increases as the monomer weight increases,

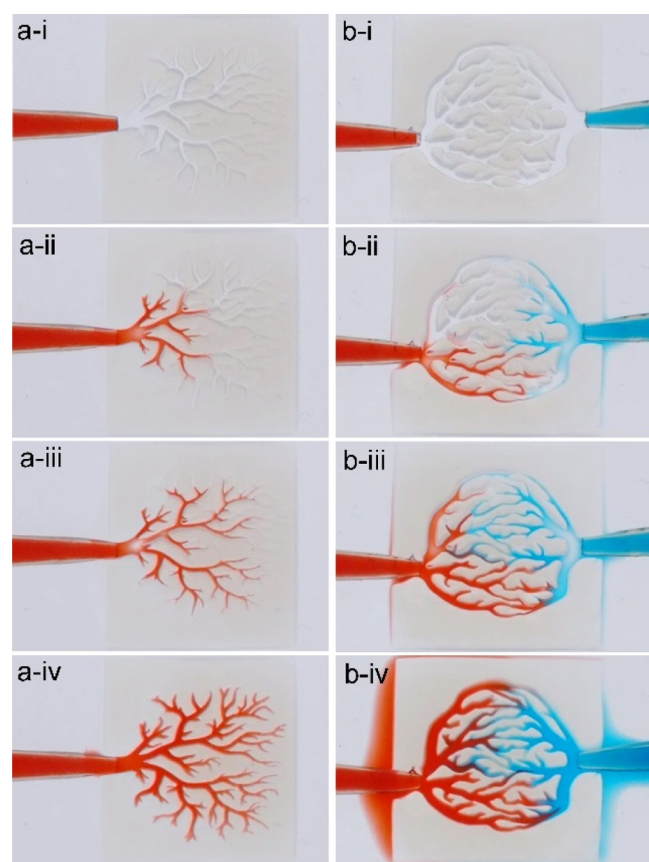


**Figure 5.** Sequential images within 2 s of perfusions show the fluid flows through the entire scaffold. (a-i–a-iv) Red dye solution is dropped at inlet of the arborescent scaffold. (b-i–b-iv) Red and blue dye solutions are dropped at the inlet and outlet, respectively, and finally merge in the center. The dye solution is driven by capillary action and fully covers all channels.

thus leading to greater biocompatibility.<sup>53</sup> However, higher porosity is generally accompanied by increased swelling and deformation in the printed scaffolds.<sup>55,56</sup> To investigate scaffold deformation after long-term immersion in DPBS, the profile of a channel in capillary network scaffold, with given widths of 75  $\mu\text{m}$ , was acquired using the laser confocal microscope. Figure 6a shows the 3D shape and the plotted profiles. Here, it is clear that the dimension, surface, and boundary morphology were maintained well even after long-term immersion. These results show that the cross-linked PEGDA exhibits negligible swelling and additional margin design or surface modification is unnecessary.

The advantages of 3D printed scaffolds featuring irregular bifurcations and intricate channels are maintained well because there is no swelling induced deformation. To assess penetration capability—which is an indicator of biocompatibility because it improves nutrient and metabolite transport—a red dye solution was used for perfusion and observation. Figure 6b displays the perfusion and penetration process in the capillary network scaffold. After 2 s of perfusion, red regions appeared across the PEGDA boundary and the penetrating regions increased on both sides of the PEGDA hurdle (Figure 6b-ii). After 30 s, the PEGDA hurdle was fully penetrated, as the penetration boundary merged in the center (Figure 6b-v). Although a high concentration of PEGDA at a small monomer weight was used, the ability to print irregular bifurcations and intricate channels with high penetration property may permit full use of the scaffold for biological applications.

**3.2. Cell Distribution and Proliferation in the Scaffolds.** To assess the biocompatibility and cell patterning ability of scaffolds, RFP-transfected A549 cells were seeded. Figure 7a,b shows the cell distribution in the capillary networks and arborescent scaffolds after attachment. A uniform cell distribution was achieved in channels wider than 30  $\mu\text{m}$ . However, clogging was observed at some terminal branches in both the arborescent and capillary network scaffolds, as shown in Figure 7c,d, taken after 36 h of culture. The main cause of clogging is flow friction, which may become significant when high density cell solution encounters subtle bifurcations. Moreover, residual water in the channels and the nonuniformity of cell suspension may also cause clogging. Despite the fact that the cell population was relatively thin in the beginning, the proliferation of new cells densely paved the channels, as is shown in Figure 7e–h.

The results of the cell seeding and culturing experiment in the printed scaffolds prove high biocompatibility and the ability to pattern cells on a multiscale level. As shown in Figure 8a, the amount of cells increased and the bifurcation was covered with cells after 36 h culture. Quantitative cell viability was then assessed to fully understand the cell proliferation process and optimize seeding conditions. A CCK-8 kit was utilized to assess cell viability at various times after cell seeding. There was a positive correlation between the absorbance measured under 450 nm and the quantity of living cells. Considering the value is 100% on 1 h, following values are normally to the value on 1 h, and the relative cell viabilities at other times are presented in Figure 8b. A high proliferation rate was achieved, which was consistent with the observed results. The cell number doubled after 12 h of culturing, while it took several days to double the cell number when cells were encapsulated inside the PEGDA hydrogel<sup>53</sup> or attached on the inner surface of the tube.<sup>14</sup> This result implies that a lower density cell solution can be used for cell seeding to reduce flow friction and improve the uniformity

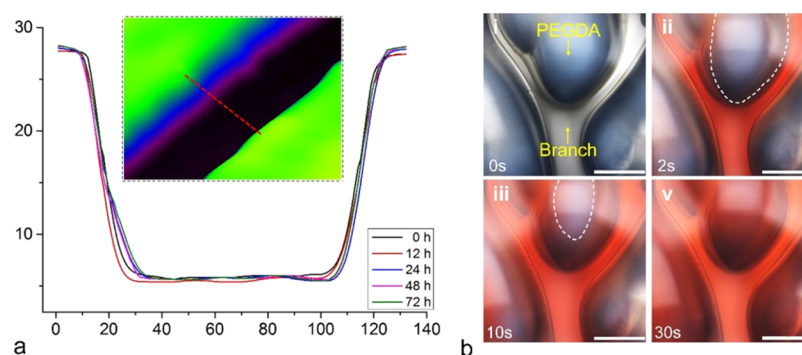


**Figure 6.** (a) Measured 3D morphology and plotted profiles under different immersion times. The red dashed line denotes the measured position. (b) Sequential microscopic images of channels in the capillary network scaffold after red dye perfusion. The white dashed line represents the change in penetration boundary. The 500  $\mu\text{m}$  wide PEGDA distance between two adjacent channels was fully penetrated after 30 s (b–v). Scale bar is 400  $\mu\text{m}$ .

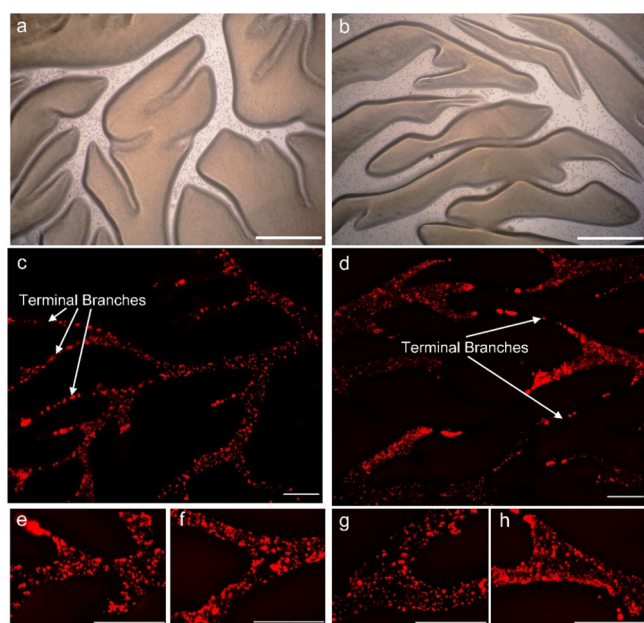


**Figure 7.** (a,b) Microscopy images of the cell distribution after attachment, taken from the 5 $\times$  objective. Fluorescent images (c,e,f) show the cell distribution in the arborescent scaffold after 36 h culture. Cells enter the terminal branches and distribute in discrete condition. Fluorescent images (d,g,h) demonstrate the cell distribution in the capillary network scaffold after 36 h culture. Images (c,d) are taken from 4 $\times$  objective and stitched together using software, and (e–h) were taken from with 10 $\times$  objective. The scale bar is 500  $\mu\text{m}$ .

of cell distribution. Although low molecular weight PEGDA was used, the high degree of polymerization for scaffold printing still has no harm to the cells. First, a high cell viability and proliferation rate after cell patterning into the scaffold have been verified. Second, for the prepared PEGDA material, a high water content is used to lower the cross-linking density during printing process, thus the substance transporting will be adequate in the printed PEGDA scaffold. Third, instead of encapsulation, the cells are seeded into the multiscale channels and attached on the glass surface, facilitating the substance exchange between cells and ECM. Therefore, this method is an indirect cell patterning and will have no UV induced harm to the cells. Through the observation and CCK-8 test, a high cell proliferation rate is observed which also demonstrated that the

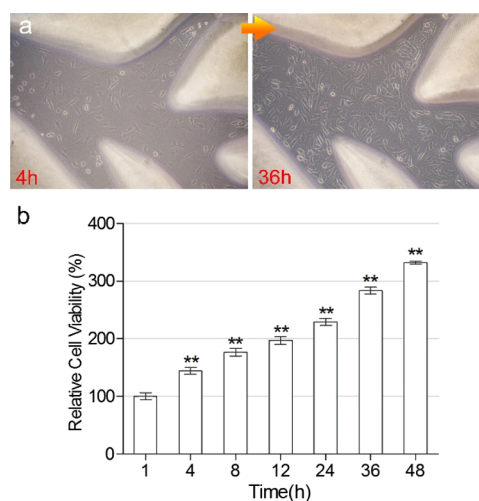


**Figure 8.** (a) Cell proliferation at 36 h in a bifurcation of capillary network scaffold. (b) Relative cell viability over 48 h. Error bars represent standard deviation and the asterisks denote differences at  $p < 0.01$ .

utilized PEGDA material with high degree of polymerization will have no harm to the cells.

#### 4. CONCLUSIONS AND FUTURE WORK

A projection-based 3D printing method was used for multiscale cell patterning by fabricating hydrogel scaffolds featuring intricate channels. The major advantage of projection-based 3D printing, allowing user defined digital masks, offers versatility to change cell patterning modes, which are crucial for reconstructing the cell microenvironment in vitro to investigate cell morphology and proliferation. In this study, hydrogel scaffolds were printed through a single step of UV exposure, which took less than 3 s. Dye solution perfusing results showed the high connectivity of printed scaffolds, which suggests that this method is capable of successfully fabricating intricate channels and offers further opportunities for cell seeding. Deformation analysis demonstrated long-term dimension stability of the hydrogel scaffolds after immersion in DPBS, and penetration test suggested the applicability of this scaffold for biotechnological applications. Next, arborescent and capillary network hydrogel scaffolds were used for cell patterning experiments. RFP-transfected A549 cell suspension was transferred at the trunk inlet of the scaffolds, and the

capillarity action-driven cell suspension then flowed into channels. Uniform cell distribution was achieved in the channels with the width larger than 30  $\mu\text{m}$ , and attachment and proliferation were observed in later culturing.

Although two biomimetic scaffolds were used to pattern cells in multiscale, the advantage of projection-based 3D printing lies in creating more complex cell patterning scaffolds with a variety of biomaterials. This is possible because of the applying of user-defined digital masks that mimic the native cellular microstructure. Future work should focus on developing the capability to pattern multiple cells using user-designed scaffolds. Direct cell patterning—by encapsulating cells into the hydrogel during printing—should be combined with seeding to increase the type to which cultured cells mimic the composition of native tissue and organs. To further reduce clogging, surface treatments (such as coating with fibronectin) should be applied to the scaffold. Because the printing ratio and resolution can be regulated by changing the distance between the DMD chip, lens, and the polymerization plane, the variable resolution of this method permits the printing of large scaffolds with intricate microstructures, which have great applicability in tissue engineering applications.<sup>57,58</sup> The possibility presented by projection-based 3D printing in terms of patterning cells in multiscale biomimetically allows us to do drug discovery, organ-on-chip, and cellular research provided with fully reconstructed cell environment.

## ■ ASSOCIATED CONTENT

### Supporting Information

The Supporting Information is available free of charge on the ACS Publications website at DOI: 10.1021/acsami.8b03867.

Using a same mask to print two scales of “ZJU” patterns under different projection ratio; relationship between height and exposure time and height verses exposure time and UV power density; masks used to print serpentine, spiral, and fractal scaffolds; and bright images of cell distribution in fractal and arborescent scaffolds (PDF)

## ■ AUTHOR INFORMATION

### Corresponding Author

\*E-mail: [yanchwang@zju.edu.cn](mailto:yanchwang@zju.edu.cn).

### ORCID

Yancheng Wang: 0000-0001-5231-6283

### Notes

The authors declare no competing financial interest.

## ■ ACKNOWLEDGMENTS

This work was supported by the National Natural Science Foundation of China (51575485), the Key Research and Development Program of Zhejiang Province (2018C01053), the Zhejiang Province Natural Science Foundation of China (LY16E05002), and the Fund for Creative Research Groups of National Natural Science Foundation of China (51521064).

## ■ REFERENCES

- (1) Discher, D. E.; Janmey, P.; Wang, Y.-L. Tissue Cells Feel and Respond to the Stiffness of their Substrate. *Science* **2005**, *310*, 1139.
- (2) Kirkpatrick, C. J.; Fuchs, S.; Unger, R. E. Co-culture Systems for Vascularization-Learning from Nature. *Adv. Drug Delivery Rev.* **2011**, *63*, 291–299.

- (3) Kaji, H.; Camci-Unal, G.; Langer, R.; Khademhosseini, A. Engineering Systems for the Generation of Patterned Co-cultures for Controlling Cell-Cell Interactions. *Biochim. Biophys. Acta* **2011**, *1810*, 239–250.

- (4) Soman, P.; Chung, P. H.; Zhang, A. P.; Chen, S. Digital Microfabrication of User-Defined 3D Microstructures in Cell-Laden Hydrogels. *Biotechnol. Bioeng.* **2013**, *110*, 3038–3047.

- (5) Hayashi, T.; Carthew, R. W. Surface Mechanics Mediate Pattern Formation in the Developing Retina. *Nature* **2004**, *431*, 647.

- (6) Lee, V. K.; Lanzi, A. M.; Ngo, H.; Yoo, S.-S.; Vincent, P. A.; Dai, G. Generation of Multi-Scale Vascular Network System within 3D Hydrogel using 3D Bio-printing technology. *Cell. Mol. Bioeng.* **2014**, *7*, 460–472.

- (7) Hou, C.; Gheorghiu, S.; Coppens, M. O.; Huxley, V. H.; Pfeifer, P. Gas Diffusion through the Fractal Landscape of the Lung: How Deep Does Oxygen Enter the Alveolar System?. *Fractals in Biology and Medicine*; Birkhäuser Basel, 2005; pp 17–30.

- (8) Wang, Y.; Yu, Z.; Mei, D.; Xue, D. Fabrication of Micro-wave Patterned Surfaces for Enhanced Cell Culturing. *Procedia CIRP* **2017**, *65*, 279–283.

- (9) Homan, K. A.; Kolesky, D. B.; Skylar-Scott, M. A.; Herrmann, J.; Obuobi, H.; Moisan, A.; Lewis, J. A. Bioprinting of 3D Convulated Renal Proximal Tubules on Perfusable Chips. *Sci. Rep.* **2016**, *6*, 34845.

- (10) Nichols, J. E.; Niles, J. A.; Vega, S. P.; Argueta, L. B.; Eastaway, A.; Cortiella, J. Modeling the lung: Design and Development of Tissue Engineered Macro- and Micro-physiologic Lung Models for Research Use. *Exp. Biol. Med.* **2014**, *239*, 1135–1169.

- (11) Kim, H. J.; Huh, D.; Hamilton, G.; Ingber, D. E. Human Gut-on-a-Chip Inhabited by Microbial Flora that Experiences Intestinal Peristalsis-like Motions and Flow. *Lap Chip* **2012**, *12*, 2165–2174.

- (12) Pati, F.; Jang, J.; Ha, D.-H.; Won Kim, S.; Rhie, J.-W.; Shim, J.-H.; Kim, D.-H.; Cho, D.-W. Printing Three-Dimensional Tissue Analogues with Decellularized Extracellular Matrix Bioink. *Nat. Commun.* **2014**, *5*, 3935.

- (13) Xu, Y.; Wang, X. Fluid and Cell Behaviors along a 3D Printed Alginate/Gelatin/Fibrin Channel. *Biotechnol. Bioeng.* **2015**, *112*, 1683–1695.

- (14) Ma, X.; Qu, X.; Zhu, W.; Li, Y.-S.; Yuan, S.; Zhang, H.; Liu, J.; Wang, P.; Lai, C. S. E.; Zanella, F.; Feng, G.-S.; Sheikh, F.; Chien, S.; Chen, S. Deterministically Patterned Biomimetic Human iPSC-Derived Hepatic Model via Rapid 3D Bioprinting. *Proc. Natl. Acad. Sci. U.S.A.* **2016**, *113*, 2206–2211.

- (15) Chang, R.; Emami, K.; Wu, H.; Sun, W. Biofabrication of a Three-Dimensional Liver Micro-organ as an in vitro Drug Metabolism Model. *Biofabrication* **2010**, *2*, 045004.

- (16) Bellan, L. M.; Singh, S. P.; Henderson, P. W.; Porri, T. J.; Craighead, H. G.; Spector, J. A. Fabrication of an Artificial 3-Dimensional Vascular Network using Sacrificial Sugar Structures. *Soft Matter* **2009**, *5*, 1354–1357.

- (17) Kim, S.; Lee, H.; Chung, M.; Jeon, N. L. Engineering offunctional, Perfusable 3D Microvascular Networks on a Chip. *Lap Chip* **2013**, *13*, 1489–1500.

- (18) Zhang, B.; Montgomery, M.; Chamberlain, M. D.; Ogawa, S.; Korolj, A.; Pahnke, A.; Wells, L. A.; Massé, S.; Kim, J.; Reis, L.; Momen, A.; Nunes, S. S.; Wheeler, A. R.; Nanthakumar, K.; Keller, G.; Sefton, M. V.; Radisic, M. Biodegradable Scaffold with Built-in Vasculature for Organ-on-a-Chip Engineering and Direct Surgical Anastomosis. *Nat. Mater.* **2016**, *15*, 669–678.

- (19) Jeon, H.; Koo, S.; Reese, W. M.; Loskill, P.; Grigoropoulos, C. P.; Healy, K. E. Directing Cell Migration and Organization via Nanocrater-Patterned Cell-Repellent Interfaces. *Nat. Mater.* **2015**, *14*, 918–923.

- (20) Kim, H. J.; Li, H.; Collins, J. J.; Ingber, D. E. Contributions of Microbiome and Mechanical Deformation to Intestinal Bacterial Overgrowth and Inflammation in a Human Gut-on-a-Chip. *Proc. Natl. Acad. Sci. U.S.A.* **2016**, *113*, E7–E15.

- (21) Wang, L.; Murthy, S. K.; Fowle, W. H.; Barabino, G. A.; Carrier, R. L. Influence of Micro-well Biomimetic Topography on Intestinal Epithelial Caco-2 Cell Phenotype. *Biomaterials* **2009**, *30*, 6825–6834.

- (22) Chien, H.-W.; Kuo, W.-H.; Wang, M.-J.; Tsai, S.-W.; Tsai, W.-B. Tunable Micropatterned Substrates based on Poly(Dopamine) Deposition via Microcontact Printing. *Langmuir* **2012**, *28*, 5775–5782.
- (23) Kobel, S. A.; Lutolf, M. P. Fabrication of PEG Hydrogel Microwell Arrays for High-Throughput Single Stem Cell Culture and Analysis. *Nanotechnology in Regenerative Medicine; Methods in Molecular Biology*; Humana Press, 2012; Vol. 811, pp 101–112.
- (24) Zawko, S. A.; Schmidt, C. E. Simple Benchtop Patterning of Hydrogel Grids for Living Cell Microarrays. *Lap Chip* **2010**, *10*, 379–383.
- (25) Hu, J.; Hardy, C.; Chen, C.-M.; Yang, S.; Voloshin, A. S.; Liu, Y. Enhanced Cell Adhesion and Alignment on Micro-wavy Patterned Surfaces. *PLoS One* **2014**, *9*, e104502.
- (26) Mei, D.; Xue, D.; Wang, Y.; Chen, S. Undulate Microarray Fabrication on Polymer Film using Standing Surface Acoustic Waves and Ultraviolet Polymerization. *Appl. Phys. Lett.* **2016**, *108*, 241911.
- (27) Zhu, W.; Qu, X.; Zhu, J.; Ma, X.; Patel, S.; Liu, J.; Wang, P.; Lai, C. S. E.; Gou, M.; Xu, Y.; Zhang, K.; Chen, S. Direct 3D Bioprinting of Prevascularized Tissue Constructs with Complex Microarchitecture. *Biomaterials* **2017**, *124*, 106–115.
- (28) Warner, J.; Soman, P.; Zhu, W.; Tom, M.; Chen, S. Design and 3D printing of Hydrogel Scaffolds with Fractal Geometries. *ACS Biomater. Sci. Eng.* **2016**, *2*, 1763–1770.
- (29) Li, S.; Liu, Y.-Y.; Liu, L.-J.; Hu, Q.-X. A Versatile Method for Fabricating Tissue Engineering Scaffolds with a Three-Dimensional Channel for Prevascularization Networks. *ACS Appl. Mater. Interfaces* **2016**, *8*, 25096–25103.
- (30) Kolesky, D. B.; Truby, R. L.; Gladman, A. S.; Busbee, T. A.; Homan, K. A.; Lewis, J. A. 3D Bioprinting of Vascularized, Heterogeneous Cell-Laden Tissue Constructs. *Adv. Mater.* **2014**, *26*, 3124–3130.
- (31) Gao, Q.; He, Y.; Fu, J.-Z.; Liu, A.; Ma, L. Coaxial Nozzle-Assisted 3D Bioprinting with Built-in Microchannels for Nutrients Delivery. *Biomaterials* **2015**, *61*, 203–215.
- (32) Buttner, U.; Sivashankar, S.; Agambayev, S.; Mashraei, Y.; Salama, K. N. Flash  $\mu$ -fluidics: A Rapid Prototyping Method for Fabricating Microfluidic Devices. *RSC Adv.* **2016**, *6*, 74822–74832.
- (33) Knowlton, S.; Yu, C. H.; Ersoy, F.; Emadi, S.; Khademhosseini, A.; Tasoglu, S. 3D-printed Microfluidic Chips with Patterned, Cell-Laden Hydrogel Constructs. *Biofabrication* **2016**, *8*, 025019.
- (34) Liu, J.; Hwang, H. H.; Wang, P.; Whang, G.; Chen, S. Direct 3D-Printing of Cell-Laden Constructs in Microfluidic Architectures. *Lap Chip* **2016**, *16*, 1430–1438.
- (35) Urrios, A.; Parra-Cabrera, C.; Bhattacharjee, N.; Gonzalez-Suarez, A. M.; Rigat-Brugarolas, L. G.; Nallapatti, U.; Samitier, J.; Deforest, C. A.; Posas, F.; Garcia-Cordero, J. L.; Folch, A. 3D-Printing of Transparent Bio-Microfluidic Devices in PEG-DA. *Lap Chip* **2016**, *16*, 2287–2294.
- (36) Gong, H.; Woolley, A. T.; Nordin, G. P. High Density 3D Printed Microfluidic Valves, Pumps, and Multiplexers. *Lap Chip* **2016**, *16*, 2450–2458.
- (37) Shallen, A. I.; Smejkal, P.; Corban, M.; Guijt, R. M.; Breadmore, M. C. Cost-Effective Three-Dimensional Printing of Visibly Transparent Microchips within Minutes. *Anal. Chem.* **2014**, *86*, 3124–3130.
- (38) Yang, Y.; Li, X.; Zheng, X.; Chen, Z.; Zhou, Q.; Chen, Y. 3D-Printed Biomimetic Super-Hydrophobic Structure for Microdroplet Manipulation and Oil/Water Separation. *Adv. Mater.* **2018**, *30*, 1704912.
- (39) Pyo, S. H.; Wang, P.; Hwang, H. H.; Zhu, W.; Warner, J.; Chen, S. Continuous Optical 3D Printing of Green Aliphatic Polyurethanes. *ACS Appl. Mater. Interfaces* **2016**, *9*, 836–844.
- (40) Manapat, J. Z.; Mangadla, J. D.; Tiu, B. D. B.; Tritchler, G. C.; Advincula, R. C. High-strength Stereolithographic 3D Printed Nanocomposites: Graphene Oxide Metastability. *ACS Appl. Mater. Interfaces* **2017**, *9*, 10085–10093.
- (41) Lin, H.; Zhang, D.; Alexander, P. G.; Yang, G.; Tan, J.; Cheng, A. W.-M.; Tuan, R. S. Application of Visible Light-based Projection Stereolithography for Live Cell-Scaffold Fabrication with Designed Architecture. *Biomaterials* **2013**, *34*, 331–339.
- (42) Palaganas, N. B.; Mangadla, J. D.; de Leon, A. C. C.; Palaganas, J. O.; Pangilinan, K. D.; Lee, Y. J.; Advincula, R. C. 3D Printing of Photocurable Cellulose Nanocrystal Composite for Fabrication of Complex Architectures via Stereolithography. *ACS Appl. Mater. Interfaces* **2017**, *9*, 34314–34324.
- (43) Hwang, H. H.; Zhu, W.; Victorine, G.; Lawrence, N.; Chen, S. 3D-Printing of Functional Biomedical Microdevices via Light- and Extrusion-Based Approaches. *Small Methods* **2018**, *2*, 1700277.
- (44) Zhang, R.; Larsen, N. B. Stereolithographic Hydrogel Printing of 3D Culture Chips with Biofunctionalized Complex 3D Perfusion Networks. *Lap Chip* **2017**, *17*, 4273–4282.
- (45) Yang, L.; Shridhar, S. V.; Gerwitz, M.; Soman, P. An in vitro Vascular Chip using 3D Printing-Enabled Hydrogel Casting. *Biofabrication* **2016**, *8*, 035015.
- (46) Nachlas, A. L.; Li, S.; Jha, R.; Singh, M.; Xu, C.; Davis, M. E. Human iPSC-derived Mesenchymal Stem Cells Encapsulated in PEGDA Hydrogels Mature into Valve Interstitial-like Cells. *Acta Biomater.* **2018**, *71*, 235–246.
- (47) Morris, V. B.; Nimbalkar, S.; Younesi, M.; McClellan, P.; Akkus, O. Mechanical Properties, Cytocompatibility and Manufacturability of Chitosan: PEGDA Hybrid-Gel Scaffolds by Stereolithography. *Ann. Biomed. Eng.* **2017**, *45*, 286–296.
- (48) Zhu, W.; Cui, H.; Boualam, B.; Masood, F.; Flynn, E.; Rao, R. D.; Zhang, Z.-Y.; Zhang, L. G. 3D Bioprinting Mesenchymal Stem Cell-Laden Construct with Core–Shell Nanospheres for Cartilage Tissue Engineering. *Nanotechnology* **2018**, *29*, 185101.
- (49) Fairbanks, B. D.; Schwartz, M. P.; Bowman, C. N.; Anseth, K. S. Photoinitiated Polymerization of PEG-Diacrylate with Lithium Phenyl-2,4,6-Trimethylbenzoylphosphine: Polymerization Rate and Cytocompatibility. *Biomaterials* **2009**, *30*, 6702–6707.
- (50) Zhang, A. P.; Qu, X.; Soman, P.; Hribar, K. C.; Lee, J. W.; Chen, S.; He, S. Rapid Fabrication of Complex 3D Extracellular Micro-environments by Dynamic Optical Projection Stereolithography. *Adv. Mater.* **2012**, *24*, 4266–4270.
- (51) Jacobs, P. F. *Rapid Prototyping and Manufacturing: Fundamentals of Stereolithography*; Society of Manufacturing Engineers Publishers: Dearborn, 1992.
- (52) Lee, K.-W.; Wang, S.; Fox, B. C.; Ritman, E. L.; Yaszemski, M. J.; Lu, L. Poly (Propylene Fumarate) Bone Tissue Engineering Scaffold Fabrication Using Stereolithography: Effects of Resin Formulations and Laser Parameters. *Biomacromolecules* **2007**, *8*, 1077–1084.
- (53) Raman, R.; Bhaduri, B.; Mir, M.; Shkumatov, A.; Lee, M. K.; Popescu, G.; Kong, H.; Bashir, R. High-Resolution Projection Microstereolithography for Patterning of Neovasculature. *Adv. Healthcare Mater.* **2016**, *5*, 610–619.
- (54) Mao, M.; He, J.; Lu, Y.; Li, X.; Li, T.; Zhou, W.; Li, D. Leaf-Templated, Microwell-Integrated Microfluidic Chips for High-Throughput Cell Experiments. *Biofabrication* **2018**, *10*, 025008.
- (55) Bertassoni, L. E.; Cecconi, M.; Manoharan, V.; Nikkhah, M.; Hjortnaes, J.; Cristino, A. L.; Barabaschi, G.; Demarchi, D.; Dokmeci, M. R.; Yang, Y.; Khademhosseini, A. Hydrogel Bioprinted Micro-channel Networks for Vascularization of Tissue Engineering Constructs. *Lap Chip* **2014**, *14*, 2202–2211.
- (56) Urrios, A.; Parra-Cabrera, C.; Bhattacharjee, N.; Gonzalez-Suarez, A. M.; Rigat-Brugarolas, L. G.; Nallapatti, U.; Samitier, J.; Deforest, C. A.; Posas, F.; Garcia-Cordero, J. L.; Folch, A. 3D-Printing of Transparent Bio-Microfluidic Devices in PEG-DA. *Lap Chip* **2016**, *16*, 2287–2294.
- (57) Zheng, X.; Smith, W.; Jackson, J.; Moran, B.; Cui, H.; Chen, D.; Ye, J.; Fang, N.; Rodriguez, N.; Weisgraber, T.; Spadaccini, C. M. Multiscale Metallic Metamaterials. *Nat. Mater.* **2016**, *15*, 1100–1106.
- (58) Zheng, X.; Deotte, J.; Alonso, M. P.; Farquar, G. R.; Weisgraber, T. H.; Gemberling, S.; Lee, H.; Fang, N.; Spadaccini, C. M. Design and Optimization of a Light-Emitting Diode Projection Micro-Stereolithography Three-Dimensional Manufacturing System. *Rev. Sci. Instrum.* **2012**, *83*, 125001.